

This work was written as part of one of the author's official duties as an Employee of the United States Government and is therefore a work of the United States Government. In accordance with 17 U.S.C. 105, no copyright protection is available for such works under U.S. Law.

Public Domain Mark 1.0

<https://creativecommons.org/publicdomain/mark/1.0/>

Access to this work was provided by the University of Maryland, Baltimore County (UMBC) ScholarWorks@UMBC digital repository on the Maryland Shared Open Access (MD-SOAR) platform.

Please provide feedback

Please support the ScholarWorks@UMBC repository by emailing scholarworks-group@umbc.edu and telling us what having access to this work means to you and why it's important to you. Thank you.



Ground-based direct-sun DOAS and airborne MAX-DOAS measurements of the collision-induced oxygen complex, O_2O_2 , absorption with significant pressure and temperature differences

E. Spinei^{1,2,5}, A. Cede^{3,2}, J. Herman^{4,2}, G. H. Mount⁵, E. Eloranta⁶, B. Morley⁷, S. Baidar^{8,9}, B. Dix⁸, I. Ortega^{8,9}, T. Koenig^{8,9}, and R. Volkamer^{8,9}

¹ESSIC, University of Maryland, College Park, MD, USA

²NASA/Goddard Space Flight Center, Greenbelt, MD, USA

³Universities Space Research Association, Greenbelt, MD, USA

⁴University of Maryland, Baltimore County, Catonsville, MD, USA

⁵Laboratory for Atmospheric Research, Washington State University, Pullman, WA, USA

⁶Space Science and Engineering Center, University of Wisconsin, Madison, WI, USA

⁷Earth Observing Laboratory, National Center for Atmospheric Research, Boulder, CO, USA

⁸Dept. of Chemistry and Biochemistry, University of Colorado, Boulder, CO, USA

⁹CIRES, University of Colorado, Boulder, CO, USA

Correspondence to: E. Spinei (espinei@wsu.edu)

Received: 17 July 2014 – Published in Atmos. Meas. Tech. Discuss.: 26 September 2014

Revised: 22 December 2014 – Accepted: 21 January 2015 – Published: 18 February 2015

Abstract. The collision-induced O_2 complex, O_2O_2 , is a very important trace gas for understanding remote sensing measurements of aerosols, cloud properties and atmospheric trace gases. Many ground-based multi-axis differential optical absorption spectroscopy (MAX-DOAS) measurements of the O_2O_2 optical depth require correction factors of 0.75 ± 0.1 to reproduce radiative transfer modeling (RTM) results for a nearly pure Rayleigh atmosphere. One of the potential causes of this discrepancy is uncertainty in laboratory-measured O_2O_2 absorption cross section temperature and pressure dependencies due to difficulties in replicating atmospheric conditions in the laboratory environment.

This paper presents ground-based direct-sun (DS) and airborne multi-axis (AMAX) DOAS measurements of O_2O_2 absorption optical depths under actual atmospheric conditions in two wavelength regions (335–390 and 435–490 nm). DS irradiance measurements were made by the Washington State University research-grade Multi-Function Differential Spectroscopy Instrument instrument from 2007 to 2014 at seven sites with significant pressure (778 to 1013 hPa) and O_2O_2 profile-weighted temperature (247 to 275 K) differences. Aircraft MAX-DOAS measurements were conducted

by the University of Colorado (CU) AMAX-DOAS instrument on 29 January 2012 over the Southern Hemispheric subtropical Pacific Ocean. Scattered solar radiance spectra were collected at altitudes between 9 and 13.2 km, with O_2O_2 profile-weighted temperatures of 231 to 244 K and nearly pure Rayleigh scattering conditions.

Due to the well-defined DS air-mass factors during ground-based measurements and extensively characterized atmospheric conditions during the aircraft AMAX-DOAS measurements, O_2O_2 “pseudo” absorption cross sections, σ , are derived from the observed optical depths and estimated O_2O_2 column densities. Vertical O_2O_2 columns are calculated from the atmospheric sounding temperature, pressure and specific humidity profiles.

Based on the ground-based atmospheric DS observations, there is no pressure dependence of the O_2O_2 σ within the measurement errors (3 %). Two data sets are combined to derive the peak σ temperature dependence of the 360 and 477 nm dimer absorption bands from 231 to 275 K. DS and AMAX-derived peak σ (O_2O_2) as a function of T can be described by a quadratic function at 360 nm and linear function at 477 nm with about $9\% \pm 2.5\%$ per 44 K rate.

Recent laboratory-measured O₂O₂ cross sections by Thalman and Volkamer (2013) agree with these “DOAS apparent” peak $\sigma(\text{O}_2\text{O}_2)$ at 233, 253 and 273 K within 3 %. Changes in the O₂O₂ spectral band shape at colder temperatures are observed for the first time in field data. Temperature effects on spectral band shapes can introduce errors in the retrieved O₂O₂ column abundances if a single room temperature $\sigma(\text{O}_2\text{O}_2)$ is used in the DOAS analysis. Simultaneous fitting of $\sigma(\text{O}_2\text{O}_2)$ at temperatures that bracket the ambient temperature range can reduce such errors.

Our results show that laboratory-measured $\sigma(\text{O}_2\text{O}_2)$ (Hermans, 2011, at 296 K and Thalman and Volkamer, 2013) are applicable for observations over a wide range of atmospheric conditions. Column densities derived using Hermans (2011) σ at 296 K require very small correction factors (0.94 ± 0.02 at 231 K and 0.99 ± 0.02 at 275 K) to reproduce theoretically calculated slant column densities for DS and AMAX-DOAS measurements. Simultaneous fitting of $\sigma(\text{O}_2\text{O}_2)$ at 203 and 293 K further improved the results at UV and visible wavelengths for AMAX-DOAS.

1 Introduction

The O₂O₂ collision complex has been widely used in remote sensing to retrieve aerosol and cloud information from spectroscopic measurements using ground-based (Wagner et al., 2002, 2004; Frieß et al., 2006; Irie et al., 2008, 2009; Clémer et al., 2010) and space instruments (Acarreta et al., 2004; Snee et al., 2008). The advantage of O₂O₂ for such measurements is that its concentration is directly proportional to the square of the oxygen concentration (Reaction R1), which is well known as a function of altitude.



The nature of molecular interactions in the O₂O₂ collisional complex is still debated (Snee et al., 2006) and the equilibrium constant, K_{eq} , is not known. As a result, only the “pseudo” O₂O₂ collisional complex can be determined, not the true concentration. After application of the ideal gas law the “pseudo” O₂O₂ column is easily calculated when atmospheric temperature, pressure and specific humidity profiles are known.

O₂O₂ absorption can be accurately measured by the differential optical absorption spectroscopy (DOAS) technique due to the presence of several absorption bands in the UV and visible parts of the spectrum (e.g., $\approx 343, 360, 380, 477, 532, 577, 630$ nm; Wagner et al., 2002), assuming availability of an accurate “pseudo” absorption cross section, σ , as a function of T and P . Laboratory measurements of σ require unrealistically long paths and/or higher pressures compared to atmospheric conditions for sufficient absorption. Despite numerous laboratory measurements of $\sigma(\text{O}_2\text{O}_2)$ in the UV and visible spectral regions (Salow and Steiner, 1934; Green-

blatt et al., 1990; Volkamer, 1996; Newnham and Ballard, 1998; Hermans, 2011; Snee and Ubachs, 2003; Snee et al., 2006; Thalman and Volkamer, 2013), the question of their applicability to atmospheric conditions remains unanswered. Only Thalman and Volkamer (2013) made $\sigma(\text{O}_2\text{O}_2)$ laboratory measurements at a pressure close to ambient (825 hPa). Their $\sigma(\text{O}_2\text{O}_2)$ at 293 K agree with the Hermans $\sigma(\text{O}_2\text{O}_2)$ at 296 K within the instrumental measurement errors. The main confusion arises from the fact that under low aerosol conditions which approach a nearly pure Rayleigh atmosphere, some ground-based multi-axis (MAX) DOAS measurements of O₂O₂ differential slant column density, ΔSCD , require a “correction factor” (CF) of about 0.75–0.89 to reproduce the $\Delta\text{SCD}(\text{O}_2\text{O}_2)$ modeled by various radiative transfer algorithms using Hermans $\sigma(\text{O}_2\text{O}_2)$ at 296 K (Table 1).

The σ dependence on temperature potentially originates from two sources: temperature dependence of K_{eq} and temperature dependence of the true absorption cross section. Pfeilsticker et al. (2001) assumed that temperature dependence is solely due to K_{eq} . Thalman and Volkamer (2013) demonstrated that the integrals of the stronger absorption lines are temperature independent, while the line shape and peak values exhibit some temperature dependence.

In this study, we investigate the pressure and temperature dependence of the cross-section peak values and line shapes using actual field DOAS measurements of O₂O₂ optical depth. We further assess the bias introduced by the temperature dependence of $\sigma(\text{O}_2\text{O}_2)$ on the DOAS fit and discuss a possible solution. Using non-scattered direct-sun (DS) photons for σ measurements is very desirable since the O₂O₂ optical depth is observed under actual atmospheric conditions and the photon path is well defined. Aircraft measurements in the free troposphere are advantageous, since they detect mainly Rayleigh scattered photons and facilitate a more straightforward comparison with radiative transfer model (RTM) calculations.

This study presents O₂O₂ “DOAS apparent” cross sections derived from ground-based DS and airborne multi-axis DOAS (AMAX-DOAS) measurements for the 335–390 and 435–490 nm wavelength ranges. Pressure dependence is evaluated from DS data collected at three sites with roughly the same O₂O₂ effective temperature (~ 266 K) and pressures of 780, 925 and 1013 hPa. Temperature dependence of $\sigma(\text{O}_2\text{O}_2)$ was examined from the ground-based DS and AMAX-DOAS measurements. DS data were collected at seven sites where $T(\text{O}_2\text{O}_2)$ ranged from 247 to 275 K. AMAX-DOAS measurements were made between 9 and 13.2 km under nearly pure Rayleigh scattering conditions with $T(\text{O}_2\text{O}_2)$ between 232 and 244 K.

The paper is organized in the following sections. Section 2 explains the methodology to calculate the normalized vertical optical depth (VOD) and peak O₂O₂ cross section using the DOAS technique. Section 3 describes the ground-based DS and AMAX-DOAS instrumentation, observation

sites and DOAS settings. Section 4 presents results. Conclusions are outlined in Sect. 5.

2 Methodology

2.1 DOAS

Differential optical absorption spectroscopy (DOAS) for weak absorbers is based on the modified Beer–Lambert law, which describes solar radiation attenuation due to molecular and aerosol absorption and scattering; see Eq. (1) (Platt, 1994; Danckaert et al., 2012). DOAS separates the strongly wavelength-dependent molecular absorption cross-section structure ($\sigma'_i(\lambda)$) of the absorbing gases from the weak wavelength dependence of the aerosol and molecular scattering and absorption (wide band extinction).

$$\ln(I_{\text{ref}}(\lambda)) - \ln(I(\lambda) - \text{offset}(\lambda)) = \underbrace{\left[\sum_s (\sigma'_i(\lambda) \cdot \Delta \text{SCD}_i) \right]}_{\text{dif. absorption}} + P_{\text{Lo}} \quad (1)$$

The DOAS technique does not require prior knowledge of Rayleigh and aerosol extinction to derive differential slant column densities (ΔSCD_i) of a gas i , since their wide band extinction can be approximated by a low-order polynomial function (P_{Lo}). Unwanted instrumental stray light is removed as an offset term, which is a function of wavelength in Eq. (1). ΔSCD_i , the low-order polynomial function and offset are simultaneously fitted by a non-linear least-squares algorithm to the difference between the logarithms of the attenuated (I) and reference (I_{ref}) spectra. The reference spectrum used in DOAS analysis is typically a solar spectrum measured by the same instrument under the lowest available slant path and abundance conditions.

The total vertical column density (VCD) measured in any DOAS observation geometry is related to ΔSCD according to Eq. (2), where SCD_{REF} is the SCD in the reference spectrum and the air-mass factor (AMF) is the photon path enhancement relative to the vertical direction.

$$\text{VCD} = \frac{\Delta \text{SCD} + \text{SCD}_{\text{REF}}}{\text{AMF}} \quad (2)$$

The AMF for ground-based DS measurements is almost wavelength independent for most solar zenith angles (SZA) and can be easily estimated using the geometrical approximation roughly equal to $1/\cos(\text{SZA})$ at $\text{SZA} < 75^\circ$. In this study we computed ground-based DS AMF accounting for Earth curvature, measurement site elevation, refraction and O₂O₂ profile calculated from measured T , P and SH profiles (modified from Cede et al., 2006). For weak absorbers with an almost constant vertical CD, such as O₂O₂, an increase in ΔSCD from DS measurements is mainly due to an increase in the photon path length (AMF). For this type of absorbers

the Langley plot method (Langley, 1881) is used to estimate SCD_{REF} .

For MAX-DOAS measurements the AMF is wavelength dependent and is a function of atmospheric composition and scattering conditions, and proper interpretation requires use of an RTM. The main complication in MAX-DOAS AMF calculations arises from insufficient knowledge of aerosol micro/macro properties and its spatial distribution. This is not a problem for the modeling of a pure Rayleigh atmosphere.

To simplify further discussion we introduce a specific notation that is followed through the remainder of the paper.

1. All quantities that exhibit strong wavelength dependence are depicted as vectors:

σ – O₂O₂ “pseudo” absorption cross section [$\text{cm}^2 \text{ molecule}^{-1}$] and

τ – O₂O₂ “pseudo” absorption optical depth, $\tau = \sigma \cdot \text{CD}$.

2. All quantities that exhibit very small or no wavelength dependence are expressed as scalars:

CD – “pseudo” column density derived from a specific fitting window [$\text{molecule}^2 \text{ cm}^{-2}$].

3. All “true” or theoretically estimated quantities from the “true” measurements are expressed using “*” superscript:

CD* – “pseudo” column density calculated from the temperature (T), pressure (P) and specific humidity (SH) profiles [$\text{molecule}^2 \text{ cm}^{-2}$],

τ^* – theoretical O₂O₂ “pseudo” absorption optical depth: $\tau^* = \sigma^* \cdot \text{CD}^*$ and

T – O₂O₂ “pseudo” profile and box AMF-weighted effective temperature [K].

4. Differential quantities are expressed using a “ Δ ” prefix.

5. Quantities integrated along the photon path (slant) are expressed using an “S” prefix; quantities integrated along the vertical direction (vertical) have a “V” prefix notation.

6. Quantities describing the reference spectrum are expressed using “REF” as subscript:

CD_{REF} – CD in the reference spectrum,

T^*_{REF} – O₂O₂ “pseudo” profile-weighted effective temperature at the reference time [K] and

τ_{REF} – O₂O₂ “pseudo” absorption optical depth in the reference spectrum.

7. The word “pseudo” is omitted while referring to O₂O₂ parameters.

Table 1. Published MAX-DOAS $\Delta\text{SCD}(\text{O}_2\text{O}_2)$ “correction factors”.

Reference	Measurement type	Measurement location and period	Wavelength fitting window, nm	Correction factor
Wagner et al. (2009)	Ground-based MAX-DOAS	Milan, Italy Sep 2003 (FORMAT-II)	360 (335–367)	~ 0.78
Cl��mer et al. (2010)	Ground-based MAX-DOAS	Beijing, China Jul 2008–Apr 2009	360 (338–370), 477 (425–490), 577 (540–588), 630 (602–645)	0.75 ± 0.10
Irie et al. (2011)	Ground-based MAX-DOAS	Cabauw, Netherlands Jun–Jul 2009 (CINDI)	360 (338–370), 477 (460–490)	Fit factor: 0.75 ± 0.10
Merlaud et al. (2011)	AMAX-DOAS, limb scanning (Safire ATR-42 aircraft)	Arctic Apr 2008 (POLARCAT France)	360 (340–370)	0.89
Vlemmix et al. (2011)	Ground-based MAX-DOAS	Cabauw, Netherlands Jun–Oct 2009 (CINDI)	477 (425–490)	0.8
Zieger et al. (2011)	Overview on ground-based MAX-DOAS	Cabauw, Netherlands Jun–Oct 2009 (CINDI)	360 (MPI) (338–370)	0.83
			477 (BIRA) (425–490)	0.75
			477 (IUPHD) (425–490)	0.8
			477 (JAMSTEC) (425–490)	0.8

8. Goodness of the linear fit between two quantities is expressed as the coefficient of determination (R^2). R^2 is rounded to two or three decimal places. For example, in case of $R^2 = 1.00$ or 1.000, less than 0.5 or 0.05 % of the variation cannot be explained by the linear model.

2.2 Pressure and temperature dependence, absorption within the planetary boundary layer

The DOAS technique can be applied to evaluate the pressure and temperature dependence of a laboratory-measured molecular absorption cross section for gases with known vertical CD*, using remote sensing atmospheric observations with well-defined AMFs. This is accomplished by evaluating the normalized τ (Eq. 3) calculated from the DOAS-fitted radiance/irradiance as a function of T or P (Wagner et al., 2002):

$$\sigma(T^*, P) = \frac{\tau}{\text{VCD}^*} = \left(\frac{\Delta S\tau + S\tau_{\text{REF}} + \tau_{\text{RESIDUAL}}}{\text{AMF}} \right) \cdot \frac{1}{\text{VCD}^*}, \quad (3)$$

where

- $\Delta S\tau$ is the DOAS-fitted O₂O₂ τ at effective measurement temperature T^* and pressure P and is equal to the product of $\Delta\text{SCD}(\text{O}_2\text{O}_2)$ and laboratory-measured σ used in the DOAS analysis: $\Delta S\tau = \Delta\text{SCD} \cdot \sigma$
- $S\tau_{\text{REF}}$ is O₂O₂ slant τ in the reference spectrum ($S\tau_{\text{REF}} = \text{SCD}_{\text{REF}} \cdot \sigma$) at T_{REF}^* and pressure P_{REF} , with

the SCD_{REF} derived using the Langley plot method from a single “reference” day at a particular site

- τ_{RESIDUAL} is the residual optical depth that is not attributed to any known absorption by the DOAS analysis at wavelength λ in each measurement.

The main assumption of the approach is that the optical density (OD) of all species absorbing in the specific wavelength window are accounted for and the residual OD is only due to the variation in the cross section of the species of interest and instrumental random noise.

Any significant differences in shape between the true O₂O₂ cross section and the fitted σ should be captured in the residual optical depth. “Broad” differences will be “masked” by the combination of polynomial and offset fits. As a result, the derived cross section in Eq. (3) is a “DOAS apparent” cross section, which might not exactly match the true cross section.

In this study, the QDOAS software package (Danckaert et al., 2012) is used to derive the ΔSCD and τ from DS measurements, and WinDOAS (Fayt and Van Roozendaal, 2001) is used for the analysis of aircraft measurements.

To evaluate a potential pressure dependence of σ , we use a DS Fraunhofer spectrum, measured at a higher altitude (lower pressure) location, as a reference spectrum to analyze DS data collected at a lower altitude (higher pressure) and the same SZA. The main requirements are high signal-to-noise ratio (SNR) in the measurements at all locations and the same $T^*(\text{O}_2\text{O}_2)$. DOAS-derived ΔSCDs are then com-

Table 2. Mean O₂O₂ vertical column density and effective temperature at the observation sites during ground-based direct-sun and aircraft MAX-DOAS measurement periods.

Site name and location	Alt./P [km hPa ⁻¹]	Observation period	Mean O ₂ O ₂ VCD* × 10 ⁴³ [molecules ² cm ⁻⁵]	AMF _{REF}	T _{REF} [*] [K]	Mean O ₂ O ₂ T* ± σ [K]
Direct sun						
TMF/JPL, CA 34.38° N 117.68° W	2.285, 779 ± 1	2–11 Jul 2007	0.767 ± 0.004	1.02	265 ± 1	264.39 ± 0.42
WSU, Pullman, WA 46.733° N 117.169° W	0.764, 913 ± 3	Sep–Nov 2007 Jul–Nov 2011	1.115 ± 0.030 1.097 ± 0.030	1.35 1.16	269 ± 1 268 ± 1	259.61 ± 4.85 262.84 ± 5.70
UAF, Fairbanks, AK 64.859° N 147.85° E	0.224, 985 ± 10	27 Mar–9 Apr 2011	1.288 ± 0.033	1.96	253 ± 1	250.35 ± 2.10
UAH, Huntsville, AL 34.725° N 86.645° W	0.223, 977 ± 3	9–18 Aug 2008	1.208 ± 0.012	1.09	271 ± 1	271.16 ± 1.02
PNNL, Richland, WA 46.3409° N 119.279° W	0.126, 1000 ± 25	15 Apr–30 Jun 2008	1.28 ± 0.03	1.06 1.09	265 ± 1	264.09 ± 5.14
GSFC/NASA, Greenbelt, MD 38.993° N 76.839° W	0.090, 1011 ± 7	May 2007 Oct 2012–Mar 2014	1.278 ± 0.02 1.299 ± 0.04	1.06 1.09	267 ± 1 266 ± 1	262.93 ± 6.51
Cabauw, Netherlands 51.971° N 4.927° E	~ 0, 1020 ± 5	16 Jun–5 Jul 2009	1.28 ± 0.02	1.14	269 ± 1	266.97 ± 2.85
Aircraft MAX-DOAS						
Subtropical Pacific Ocean 29.7–29.9° S 92.4–92.1° E	9–13.2, 321–174	18:06–18:30 UTC 29 Jan 2012	1.29	VIS: 0.98 UV: 0.89	VIS: 252.4 ± 0.2 UV: 247.6 ± 0.2	VIS: 236.3 ± 5.2 UV: 238.6 ± 3.2

pared to ΔSCD^* estimated from T , P and SH profiles at the corresponding sites. We do not expect to detect any line broadening by using this analysis due to the large spectral width of the O₂O₂ spectral bands (> 5 nm).

This approach can be used to detect whether higher absorption is observed within the planetary boundary layer (PBL) under conditions that are probed by ground-based MAX-DOAS observation geometry. To “simulate” MAX-DOAS absorption within the PBL at different elevation angles relative to a zenith spectrum, we analyze DS spectra collected at an approximately sea-level site (0.1 km above sea level, a.s.l.) relative to the reference spectra collected

over the higher altitude sites (2.3 and 0.8 km a.s.l.) as a function of SZA (20, 60, 75, 80, 83°). Since both the reference and analyzed spectra are measured at the same SZA but at two different site altitudes, the resulting $\Delta\text{SCD}(\text{O}_2\text{O}_2)$ is $\text{SCD}(\text{O}_2\text{O}_2)$ within the PBL only (2.2 and 0.7 km). The AMF values within the PBL absorbing layer for the tested SZA range are between 1.1 and 9.

To evaluate the temperature dependence of σ , both ground-based DS and AMAX-DOAS data are used. For DS observations, a reference Fraunhofer spectrum measured at the smallest SZA is applied to the data collected at the same site. For the AMAX-DOAS measurements, a spectrum, col-

Table 3. DOAS analysis parameters used in direct-sun and aircraft MAX-DOAS analysis.

	Direct sun		Aircraft MAX-DOAS	
Fitting window	338–388 nm ^a 350–385 nm ^b	435–490 nm	350–387.5 nm Gap: 366–374.5 nm	445–485 nm
BrO	223 K, Fleischmann et al. (2004)	–	228 K, Wilmouth et al. (1999)	–
HCHO	298 K, Meller and Moortgat (2000)	–	298 K, Meller and Moortgat (2000)	–
H ₂ O	–	296 K, HITEM, Rothman (2010)	–	296 K, HITEM, Rothman (2010) and lab ^c
O ₃	228 and 243 K, Daumont et al. (1992)		223 K, Bogumil (2003)	
NO ₂	linear model, Vandaele et al. (2003)		220 K, Vandaele et al. (1998)	
O ₂ O ₂	296 K, Hermans (2011)		296 K, Hermans (2011) 203 and 293 K, Thalman and Volkamer (2013)	
Ring	–		Ring at 250 K from reference Ring at 220 K from second reference	
Polynomial order	4 ^a , 3 ^b		5	
Offset	slope		slope	

^a Spectra with U340 filter.^b Spectra without any filters.^c Cross section recorded with AMAX-DOAS instrument at room temperature through an LED cavity system in the laboratory (Thalman and Volkamer, 2013).

lected at ceiling altitude (13.2 km) pointing 10° above horizontal direction (EA 10°), is used as a reference Fraunhofer spectrum.

3 Data description, DOAS and radiative transfer settings

3.1 Direct-sun measurements

DS spectra were measured by the Washington State University (WSU) Multi-Function Differential Spectroscopy Instrument (MFDOAS) (Herman et al., 2009) in the wavelength region 282–498 nm at seven sites: JPL-Table Mountain Facility, CA (TMF); University of Alabama, Huntsville (UAH); Cabauw, Netherlands; University of Alaska in Fairbanks (UAF); Washington State University, Pullman, WA; Pacific Northwest National Laboratory (PNNL), Richland, WA; and Goddard Space Flight Center (GSFC/NASA), Greenbelt, MD. Temperature, pressure and specific humidity profiles were composed for each site from the following sources to ensure consistent vertical CD* calculation from the surface to the top of the atmosphere:

- surface pressure, temperature and relative humidity measured by a Vaisala Weather Transmitter WXT520

- radio soundings launched at nearby sites twice a day (00:00 and 12:00 UTC, available at <http://weather.uwyo.edu/upperair/sounding.html>); during some field campaigns frequent ozonesonde measurements were also available (UAF, TMF, UAH)
- *T*, *P* and SH profiles (instantaneous 6 h) Modern Era Retrospective-Analysis for Research and Applications (<http://gmao.gsfc.nasa.gov/merra/>).

Table 2 summarizes average VCD*(O₂O₂) and *T** calculated for each site from the *T*, *P* and SH profiles.

The MFDOAS instrument combines measurements of DS irradiance and scattered sun radiance (MAX-DOAS). DS photons are collected by a telescope with a 1.4° field of view (FOV) and are guided through the 8 cm diameter Spectralon integrating sphere. The integrating sphere assures uniform illumination of the spectrometer optics and minimizes the effect of FOV pointing inaccuracy. A modified 300 mm focal length single-pass Czerny–Turner spectrometer (Acton Research, Inc., SpectraPro-2356) is used to disperse light. A 400 groove per mm ruling grating blazed at 400 nm is installed in the grating turret. Light enters the spectrometer through a 100 μm slit. The internal spectrograph baffling masks have been substantially modified from the commercial version to eliminate re-entrant light and scattering artifacts. A charge-coupled device (CCD) (Princeton Instruments PIXIS:

2KBUV) is used to detect the spectrally dispersed light. It has an enhanced UV sensitivity due to back illumination and UV coating. The imaging area is composed of 512 rows by 2048 columns of square pixels ($13.5 \times 13.5 \mu\text{m}^2$). MFDOAS has an average spectral resolution of 0.83 nm with a sampling of 7.83 pixels per full width at half maximum (FWHM). Typical averaging time from many exposures in DS mode is 1 min.

MFDOAS spectra were analyzed in two wavelength regions, 335–390 and 435–490 nm, to evaluate the ~ 360 and 477 nm O₂O₂ absorption lines. Table 3 lists all fitting parameters and laboratory-measured higher resolution trace-gas molecular absorption cross sections used in DOAS analyses after convolution with the MFDOAS instrument transfer function. All cross sections were fitted as non-differential cross sections to remove dependence on the polynomial order used to estimate cross-section broadband absorption. To evaluate DOAS errors associated with the fitting parameters we varied the wavelength fitting windows (435–485, 435–490, 450–485, 350–385, 338–370, 335–390 nm), polynomial order (3, 4 and 5) and offset order (0 and 1).

A single, site-specific, reference Fraunhofer spectrum was selected to analyze all the data available at the corresponding site (for the same instrument configuration). This reference spectrum was calculated as an average of spectra collected during a 30 min interval around a small SZA. Since vertical CD*(O₂O₂) can vary by a few percent during a particular day due to diurnal pressure/temperature changes, only days with relatively constant surface P were selected as reference days. The Langley plot method to derive SCD_{REF} was applied only to the DS spectra collected during these reference days.

Pressure dependence was examined by using a reference spectrum measured at TMF located at 2.3 km above sea level with surface pressure of 780 hPa to analyze data collected at WSU (925 hPa) and GSFC (1013) with $T^*(\text{O}_2\text{O}_2) \approx 266$ K.

3.2 AMAX-DOAS measurements of O₂O₂ in a nearly pure Rayleigh atmosphere

The TORERO field experiment (Tropical Ocean Troposphere Exchange of Reactive halogen species and Oxygenated VOC, January–February 2012) provided an opportunity to measure and assess O₂O₂ absorption in a Rayleigh atmosphere by means of the University of Colorado airborne MAX-DOAS instrument (Baidar et al., 2013). TORERO deployed a unique selection of chemical in situ and remote sensing instruments aboard the National Science Foundation V aircraft over the eastern Pacific Ocean. We have measured ambient temperature, pressure, water vapor and ozone (all by in situ sensors), aerosol size distributions by an ultra-high-sensitivity aerosol spectrometer and temperature profiles by a microwave temperature profiler (MTP) (Denning et al., 1989; Lim et al., 2013), and aerosol extinction profiles by high-spectral-resolution LIDAR (HSRL; Eloranta et al., 2008). Four cameras provide information on cloudiness: forward,

sideways and below the aircraft. Research flight 05 (RF05) was conducted on 29 January 2012 from/to Antofagasta, Chile, over the Southern Hemispheric subtropical Pacific Ocean, where the aircraft probed very clear air during a case study from 18:06 to 18:30 UTC (9 to 13.2 km altitude; SZA of 12.4 to 12.0°; 92.4–92.1° E/29.7–29.9° S). The ambient temperature varied from 235.4 to 214.3 K. The corresponding O₂O₂ effective temperatures, calculated for 360/477 nm using box AMFs and measured T , P and SH, ranged from 243.4/239.3 to 235.3/232.4 K (see Table 2). The camera data show only sparsely scattered boundary-layer clouds. The aerosol extinction profile measured by the HSRL at 532 nm showed sub-Rayleigh aerosol extinction values above the aircraft. The aerosol content in the stratosphere was nominally zero, i.e., the measured aerosol backscatter cross section is too small to derive any extinction values. Below the aircraft, aerosol extinction was sub-Rayleigh above 1.5 km and agreed very well (better 0.01 km^{-1}) with Mie calculations below 1.5 km (see Fig. 1). Mie calculations were constrained by measured size distributions and used to better quantify the low aerosol extinction values in the free troposphere as well as to estimate the wavelength dependence of aerosol extinction at the O₂O₂ wavelengths. The mean aerosol number density between 9 and 13.2 km was $5.8 \pm 1.7 \text{ cm}^{-3}$. The average aerosol size distribution over this altitude range had an effective radius: $R_e = 0.11 \pm 0.02 \mu\text{m}$. Mie code was initiated assuming a constant refractive index, n , at all sizes and wavelength dependencies as described in Massie and Hervig (2013). Sensitivity studies varied $n \sim 1.55$ (sea salt), ~ 1.30 (ice) and ~ 1.56 (mineral dust). The aerosol extinction values (sea salt) averaged between 9 and 13.2 km are $4.6 \times 10^{-4} \text{ km}^{-1}$ (532 nm), $5.2 \times 10^{-4} \text{ km}^{-1}$ (477 nm) and $6.7 \times 10^{-4} \text{ km}^{-1}$ (360 nm), respectively. These numbers are 1 to 2 orders of magnitude lower than the extinction due to molecular (Rayleigh) scattering at the O₂O₂ wavelengths (see Fig. 1). The atmospheric radiation state can be described in good approximation as a Rayleigh atmosphere.

AMAX-DOAS measures scattered sunlight spectra from well-defined lines of sight. The limb-scanning telescope has a FOV of 0.17° and is actively angle-stabilized to better 0.2° accuracy in real time (Baidar et al., 2013; Dix et al., 2013). Two synchronized spectrograph–detector units (Acton SP2150/PIXIS400B CCD) simultaneously observed the spectral ranges from 330 to 470 nm (0.7 nm FWHM optical resolution) and 430 to 680 nm (1.2 nm FWHM optical resolution). $\Delta\text{SCD}(\text{O}_2\text{O}_2)$ were retrieved by application of a non-linear least-squares DOAS fitting routine using the WinDOAS software package (Fayt and van Roozendaal, 2001) for two wavelength windows: 350–387.5 nm (with a gap between 366 and 374.5 nm to minimize ring effect) and 445–485 nm using (1) the Hermans cross section at 296 K (Hermans, 2011) and (2) the Thalman and Volkamer cross sections at 293 and 203 K (Thalman and Volkamer, 2013). These analysis settings are optimized to retrieve robust ΔSCDs over the wide range of atmospheric conditions encountered during

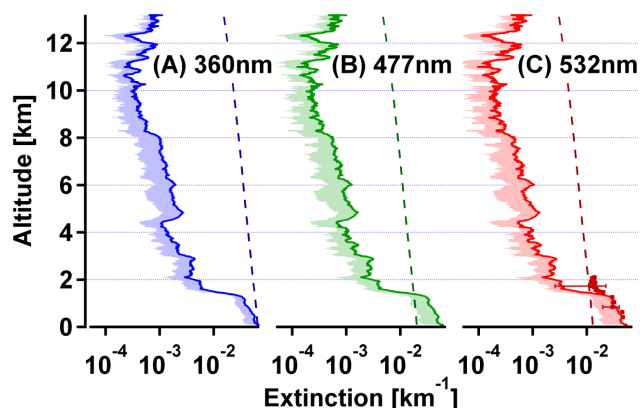


Figure 1. Vertical profiles of aerosol extinction at (a) 360 nm, (b) 477 nm and (c) 532 nm during the AMAX-DOAS case study (solid lines) and HSRL-measured extinction at 532 nm (red squares); Mie calculations constrained by measured size distributions assuming “*n*” of sea salt; sensitivity studies assuming “*n*” of pure water (shading); extinction from Rayleigh scattering for air densities calculated from measured temperature, pressure and water vapor profiles (dashed lines).

a typical 8 h flight time. A summary of analysis settings and cross sections used can be found in Table 3. One spectrum collected at 13.2 km altitude was used as a reference Fraunhofer spectrum to analyze all data (see Table 2). The reference elevation angle is upward looking (EA 10°) to minimize the slant column amount contained in the reference, SCD_{REF}. Spectra were measured at EA 0° (i.e., horizontal and parallel to flight altitude) during ascent; further three upward angle scans (1°, 2°, 5°) at constant flight altitude (13.2 km) were included in the analysis.

Radiative transfer calculations were performed with McArtim (Deutschmann et al., 2011), a fully spherical Monte Carlo RTM, for 360 and 477 nm. Radiation fields were constrained by in situ pressure, temperature, water vapor, ozone, MTP temperature profiles and stratospheric profiles of NO₂ and O₃ taken from the Real-time Air Quality Modeling System (RAQMS) (Piers et al., 2007). The O₂O₂ vertical profile was calculated as the square of the O₂ concentration based on measured temperature and pressures and corrected for water vapor concentration. Ocean surface albedo was set to 5 % at 360 nm and to 8 % at 477 nm. Solar and observation geometry were input variables for the RTM.

4 Results and discussion

4.1 O₂O₂ reference slant optical depth in direct sun and AMAX-DOAS measurements

Estimation of $S\tau_{\text{REF}}$ in Eq. (3) requires determination of SCD_{REF} from the ground-based DS and AMAX-DOAS data. SCD_{REF} is calculated from the DOAS-fitted ΔSCD using Hermans (2011) $\sigma(\text{O}_2\text{O}_2)$ at 296 K by applying the Langley

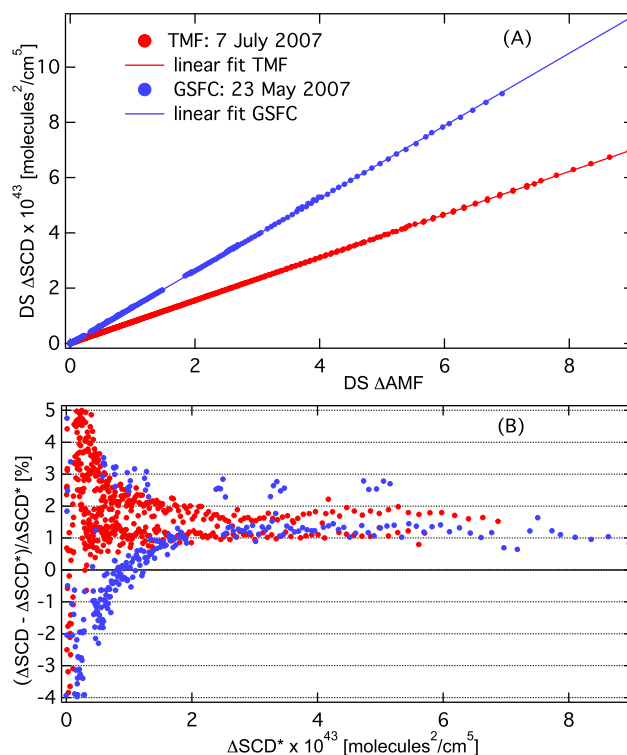


Figure 2. (a) Linear regression between MFDOAS-measured direct-sun ΔSCD and ΔAMF (Langley plot) to derive SCD(O₂O₂) in the reference spectra at TMF and GSFC sites. Correlation is calculated using the least-squares method. R^2 of the linear fit is > 0.9995 . Slope represents estimation of SCD_{REF} from 435–490 nm fitting window and DOAS fitting settings summarized in Table 3; (b) difference between DS-measured ΔSCD and calculated ΔSCD^* as a function of ΔSCD^* for data from (a).

plot method. SCD_{REF} is then multiplied by σ to determine $S\tau_{\text{REF}}$.

4.2 Direct-sun measurements

SCD_{REF} was calculated from the DS measurements at each site in the UV and visible fitting windows using the Langley plot method. Examples of the Langley plots for the reference data collected over the TMF (high-altitude unpolluted site) and GSFC (~sea level polluted site) analyzed in 435–490 nm, with the settings described in Table 3, are presented in Fig. 2. The linear regression analysis presented in Fig. 2 is similar at all sites and shows high correlation between the DS ΔSCD and ΔAMF , with R^2 of 1.000 for the visible wavelength region and better than 0.980 for the UV. The final error in the SCD_{REF} derived from the UV and visible wavelength windows was determined as 1 standard deviation of SCD_{REF} calculated from ΔSCDs with different DOAS fitting parameters (e.g., polynomial order, offset order, fitting window boundaries). The estimated relative error in measured SCD_{REF} from the visible wavelength region is about 0.8 %

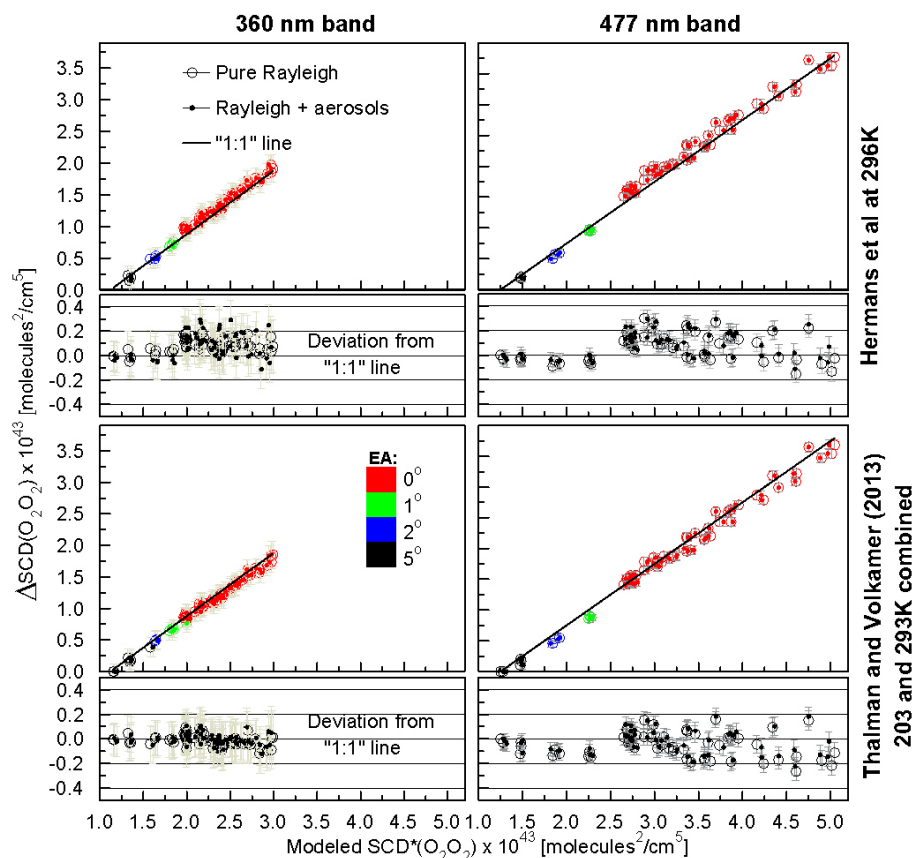


Figure 3. Measured Δ SCDs at 360 nm (left panel) and 477 nm (right panel) vs. modeled $\text{SCD}^*(\text{O}_2\text{O}_2)$ for a pure Rayleigh atmosphere and with aerosol profile using fitting parameters outlined in Table 3. Upper panel presents data using Hermans (2011) $\sigma(\text{O}_2\text{O}_2)$ at 296 K; lower panel shows combined data from Thalman and Volkamer (2013) at 203 and 293 K with their corresponding deviations from the “1 : 1” line. Color code represents AMAX viewing elevation angles of individual data points. Error bars are based on twice-fit residual RMS to represent fit accuracy.

and from the UV wavelengths about 2.4 %. Agreement between the derived SCD_{REF} from DS measurements and calculated $\text{SCD}^*_{\text{REF}}$ is temperature dependent and ranges from 1.5 % at 265 K to 3 % at 253 K.

4.3 AMAX-DOAS measurements

SCD_{REF} in the AMAX reference Fraunhofer spectrum, measured at 13.2 km and 10° EA, was calculated from the linear correlation between the measured Δ SCD and modeled SCD^* at 360 and 477 nm, assuming pure Rayleigh scattering conditions (Fig. 4, upper panel). SCD^* accounted for an altitudinal dependence of vertical $\text{CD}^*(\text{O}_2\text{O}_2)$. The slant column amount contained in the reference is the absolute value of the intercept. Linear regression parameters are summarized in Table 4. The modeled SCD_{REF} values agree with the SCD_{REF} inferred from the measurements within 1.7 % at 360 nm and 1.6 % at 477 nm. The slope of the linear correlation is expected to be unity if there is no temperature dependence of $\sigma(\text{O}_2\text{O}_2)$ and atmospheric conditions are correctly described by the model. Given the small temperature dependence of the

O₂O₂ cross-section shape (Thalman and Volkamer, 2013), some deviation from “1” is expected while fitting $\sigma(\text{O}_2\text{O}_2)$ at a single T . The observed divergences from “1” are 2.9 % at 360 nm and 1.6 % at 477 nm.

To evaluate the effect of aerosol extinction below the aircraft on the linear correlation between the measured Δ SCD and estimated SCD^* (SCD_{REF} and slope), we recalculated AMFs and SCD^* including the extinction profiles derived from Mie theory. In the RTM, aerosols are described by single scattering albedo (0.97 at 360 nm, 0.98 at 477 nm) and g parameter (0.75–0.7 for 0–13 km). The extinction profile is taken from the Mie calculations for the sea salt case (see Fig. 1). For the aerosol scenario, agreement between the measured SCD_{REF} and estimated $\text{SCD}^*_{\text{REF}}$ slightly improves (0.9 % at 360 nm and 0.8 % at 477 nm), but slope deviations from “1” increase to 5.2 ± 5 % at 360 nm and 2.6 ± 1 % at 477 nm.

Table 4. Linear correlation parameters between AMAX-DOAS $\Delta\text{SCD}(\text{O}_2\text{O}_2)$ using Hermans (2011) σ (296 K)/Thalman and Volkamer (2013) σ (203 and 293 K) and McArtim modeled SCDs.

	Pure Rayleigh scattering		Rayleigh with aerosols Scattering	
Fitting window, model wavelength [nm]	350–387.5, 360	445–485, 477	350–387.5, 360	445–485, 477
R^2	1.00/0.98	1.00/1.00	0.99/0.98	1.00/0.99
Slope*	$1.029 \pm 0.049/$ 0.957 ± 0.044	$1.016 \pm 0.01/$ 0.986 ± 0.008	$1.052 \pm 0.050/$ 0.978 ± 0.045	$1.026 \pm 0.01/$ 0.996 ± 0.01
Intercept $\times 10^{43}$ [molecules ² cm ⁻⁵]	$1.13 \pm 0.11/$ 1.07 ± 0.09	$1.23 \pm 0.03/$ 1.25 ± 0.03	$1.18 \pm 0.08/$ 1.12 ± 0.08	$1.27 \pm 0.03/$ 1.29 ± 0.03
Modeled $\text{SCD}_{\text{REF}} \times 10^{43}$ [molecules ² cm ⁻⁵]	1.15	1.25	1.17	1.28

* \pm standard deviation

4.4 $\sigma(\text{O}_2\text{O}_2)$ pressure dependence (absorption within PBL) from ground-based DS measurements

To investigate the effect of pressure on $\sigma(\text{O}_2\text{O}_2)$, we used the DS Fraunhofer spectra collected over TMF at 2.3 km a.s.l. (7 July 2007) and over WSU at 680 m a.s.l. (11 September 2007) as reference spectra to analyze the spectra measured over GSFC at 90 m a.s.l. (23 May 2007) with similar T_{eff} (267 ± 2 K). About 40 % (0.513×10^{43} molecules² cm⁻⁵) of total O₂O₂ column is located between TMF and GSFC altitudes (from 780 to 1011 hPa) and less than 20 % (0.206×10^{43} molecules² cm⁻⁵) is located between WSU and GSFC altitudes (from 925 to 1011 hPa). Both the reference and analyzed spectra were measured at the same SZA but at the two different locations. This DS DOAS analysis detects only O₂O₂ absorption within the lowest 2.2 km in case of TMF/GSFC sites or 680 m in case of WSU/GSFC sites for varying layer AMF. Note that SNR of the reference and analyzed spectra both decrease with increasing SZA, and so the residual OD is increasing at a “faster rate” compared to the analysis when a single noon reference is used to analyze spectra collected at all SZA. We have limited the maximum SZA to 83° to ensure that the observed residual OD RMS is less than 5×10^{-4} .

Figure 4 shows DOAS fitting OD results for 20, 60, 75, 80, 83° SZA in the 435–490 nm wavelength window using Hermans (2011) $\sigma^*(\text{O}_2\text{O}_2)$ at 296 K when TMF references were used to analyze GSFC spectra. The agreement between the ΔSCD^* and DOAS-retrieved ΔSCD between the two sites at 780 and 1011 hPa is within 3 % for all cases. The DOAS residual OD exhibits both wavelength and AMF-dependent structure, but because the SNR of the DS measurements is AMF dependent, this could be either an instrumental or atmospheric artifact. However, the observed high frequency of this residual OD spectrum is unlikely to be related to a pres-

sure effect on the O₂O₂ cross section. Residual spectral OD RMS at 20° SZA is 9.6×10^{-5} and at 83° SZA is 2.7×10^{-4} . This residual OD is smaller or comparable to MAX-DOAS measurements. A comparison of AMF-normalized OD spectral residuals retrieved from TMF data using the TMF reference, and with GSFC spectra using both TMF and GSFC reference spectra, shows similar spectral structure between 470 and 485 nm with 1.4×10^{-4} peak to valley magnitude (Fig. 4c). This is probably related to the difference between the “true” cross section at 267 K and Hermans (2011) cross section at 296 K.

Similar results were obtained when DS data from the WSU site were used as the reference to derive O₂O₂ absorption from the GSFC data. In this case, retrieved absorption is within the lowest 680 m. Due to such small ΔVCD^* (half of the TMF-GSFC value), we considered only data with AMF from 3 to 9. The agreement between the measured ΔSCD and ΔSCD^* is within 2–4 % for all cases. Figure 4 shows the DOAS-fitted $\sigma(\text{O}_2\text{O}_2)$ and OD residuals for absorption within the 680 m at layer AMF ≈ 8.4 and $\Delta\text{SCD}^* = 1.722 \times 10^{43}$ molecules² cm⁻⁵.

Performing a similar analysis as a function of SZA in the UV from the same 282–498 nm spectra was not possible due to low SNR of UV irradiance at high SZA. However, for UV measurements at SZA 19° over GSFC and 42° over WSU, the agreement between the measured and estimated ΔSCD is within 3 % using settings outlined in Table 3. The OD spectral residual RMS is 2.8×10^{-4} over GSFC and 2.7×10^{-4} over WSU. There is a broad residual structure between 365 and 373 nm with a peak-to-valley optical depth of $\sim 1 \times 10^{-3}$ when the TMF reference spectrum is used to analyze GSFC/WSU data. However, this structure is not present in the GSFC and WSU data when the reference spectra from the corresponding sites are used. The source of this structure is unclear at this point.

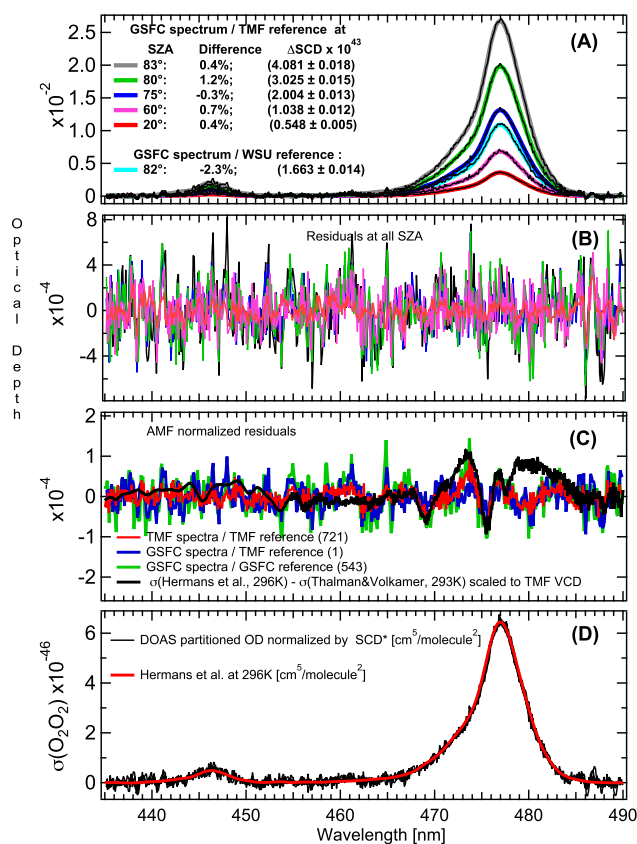


Figure 4. O₂O₂ optical depth derived from the DS MFDOAS spectra (no filters) collected over GSFC, Greenbelt, MD (1013 hPa, 23 May 2007), relative to the reference spectrum collected over TMF (780 hPa, 7 July 2007) and WSU, Pullman, WA (925 hPa, 11 September 2007), at approximately the same solar zenith angles and the Teff 266 K in the visible spectral window: (a) DOAS fitting for each SZA and respective errors in comparison with the theoretically estimated ΔSCD ; (b) residual optical depth at all SZA; (c) “DOAS apparent” O₂O₂ absorption cross section derived from the data in panel (a); (d) residual optical depth normalized by AMF.

We conclude that $\sigma(\text{O}_2\text{O}_2)$ does not exhibit any pressure sensitivity between 780 and 1011 hPa within typical DOAS instrumental and fitting errors. There is a good agreement (2–4 %) between observed and calculated ΔSCD within PBL when DS PBL-only AMF approach MAX-DOAS AMF.

4.5 Temperature dependence of observed $\tau(\text{O}_2\text{O}_2)$

Since no pressure dependence was observed between 780 and 1013 hPa, we combined data from all sites for ground-based DS and AMAX-DOAS measurements to determine the temperature dependence of $\sigma(\text{O}_2\text{O}_2)$. $\tau(\text{O}_2\text{O}_2)$ values from DS measurements (Eq. 3) were averaged to produce single daily values. Vertical CD* calculated from T , P and SH profiles were interpolated on a DS daily time grid. The AMAX-DOAS data were binned and averaged within 2 K increments to derive vertical column densities. VCD* was calculated

from simultaneous in situ temperature and pressure measurements, corrected by in situ water vapor data. Above the aircraft, the temperature profile was extended using MTP data and RAQMS model pressure.

Figure 5 provides an example of the AMAX-DOAS spectral fit in the UV and visible windows for O₂O₂ effective temperatures of 239.7 ± 0.4 K at 360 and 234.8 ± 0.5 K at 477 nm using Hermans (2011) $\sigma(\text{O}_2\text{O}_2)$ at 296 K. When only a single temperature σ is fitted, systematic structures remain in the DOAS-fitted residual optical depths, apparent both in UV and visible windows. This is a clear reflection of temperature-dependent band-shape changes in $\sigma(\text{O}_2\text{O}_2)$, as described by Thalman and Volkamer (2013), that a single cross section at 296 K cannot account for during the fit.

Figure 6 shows vertical optical depths at 360 (a) and 477 nm (b), derived from DS and AMAX-DOAS measurements over all sites and normalized by VOD*. Normalization by VOD* is applied to remove differences in spectral resolution between the MFDOAS and AMAX-DOAS instruments. This also allows detection of any systematic differences in DOAS-retrieved $\tau(\text{O}_2\text{O}_2)$ as a function of temperature relative to the fitted Hermans et al. $\sigma(\text{O}_2\text{O}_2)$ at 296 K.

Ground-based DS measurements indicate a clear increase in DOAS-normalized VOD at 360 and 477 nm, at a rate of 5 ± 2 % per 30 K, from 275 to 247 K. Similar trends are observed over all DS sites regardless of their significant differences in NO₂, HCHO, H₂O and O₃ columns. The spread of the derived “DOAS-apparent” peak $\sigma(\text{O}_2\text{O}_2)$ of the 477 nm band (± 1 %) is within the error of VCD*(O₂O₂) from T , P and SH profiles (1.6 %). More variability is observed for the peak $\sigma(\text{O}_2\text{O}_2)$ of the 360 nm band (± 2 %) due to a lower SNR in the UV part of the spectrum and higher sensitivity to the DOAS fitting parameters. The AMAX-DOAS data exhibit a similar trend when using the Hermans (2011) cross section between 231 and 244 K.

Figure 7 shows the comparison between O₂O₂ peak $\sigma(T^*)$ of the 360 and 477 nm bands derived from ground-based DS and AMAX-DOAS measurements using Hermans (2011) σ (this work) and published σ values. Peak values derived in this work and Thalman and Volkamer (2013) agree within the DS and AMAX-DOAS errors for both spectral bands at 233, 253 and 273 K. Error budgets for the DS and AMAX-DOAS O₂O₂ peak $\sigma(T)$ of 360 and 477 nm bands are summarized in Table 5 (for the detailed discussion of errors see Sect. 4.5). Sneepe et al. (2006) peak $\sigma(230$ K) at 477 nm is 18 % lower than the observed values in this study. Osterkamp et al. (1998) and Wagner et al. (2002) measured O₂O₂ absorptions under atmospheric conditions with the Osterkamp et al. peak $\sigma(256$ K) at 477 nm, agreeing with the results presented here within the measurement errors. Wagner et al. (2002) O₂O₂ peak $\sigma(242$ K) is 25 and 12 % larger than the derived values in this study for 360 and 477 nm, respectively.

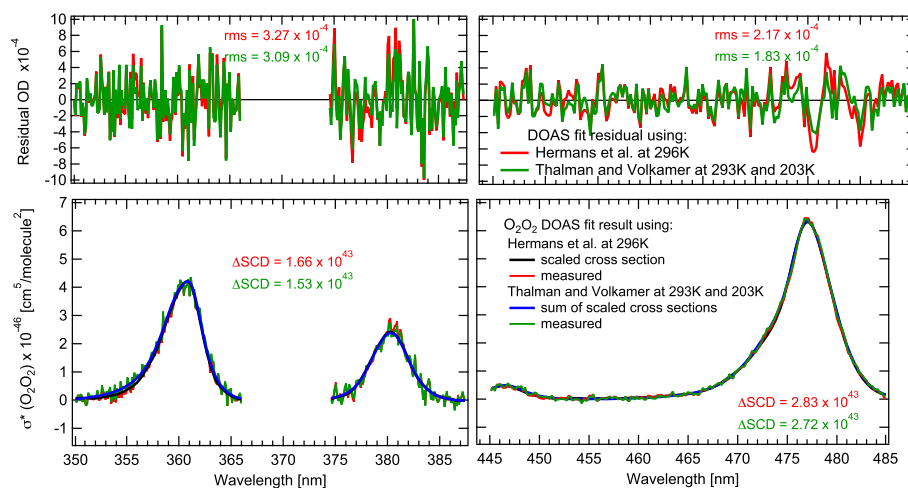


Figure 5. AMAX-DOAS spectral fit examples in UV and visible windows fitting (top) only one O₂O₂ cross section – Hermans (2011) at 296 K – and (bottom) two O₂O₂ cross sections – Thalman and Volkamer (2013) at 203 and 293 K. The effective O₂O₂ temperatures for the displayed spectra are 239.7 ± 0.4 K at 360 and 234.8 ± 0.5 K at 477 nm.

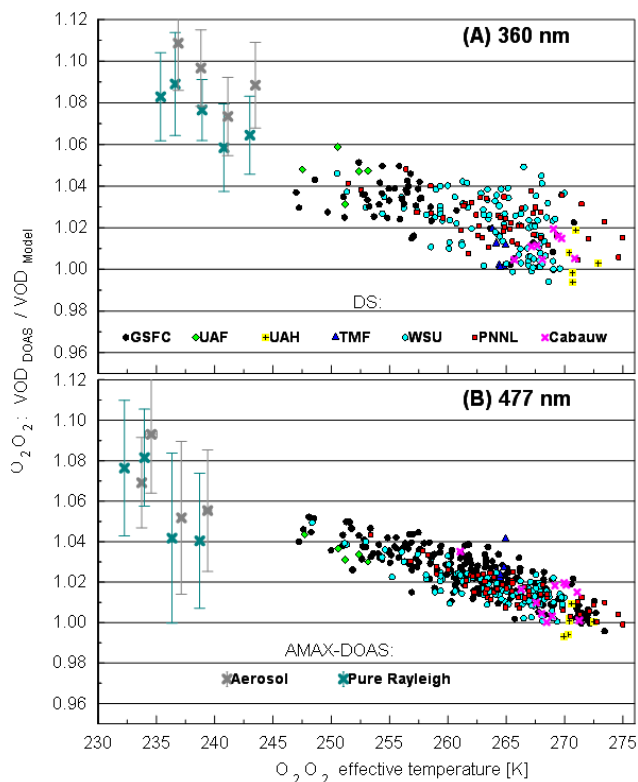


Figure 6. Vertical optical depth at 360 (a) and 477 nm (b), derived from DS and AMAX-DOAS measurements over all sites and normalized by the VOD* calculated from sonde/measured/model temperature, pressure and specific humidity profiles as a function of O₂O₂ effective temperature. AMAX-DOAS data are averaged and binned for 2 K increments for a pure Rayleigh atmosphere and including aerosols. Table 3 lists DOAS settings.

Table 5. Error budget of the 360 and 477 nm band peak O₂O₂ $\sigma(T)$ derived from DS and AMAX-DOAS measurements.

Error source	Error peak of 360 nm band	Error peak of 477 nm band
Direct-sun DOAS		
O ₂ O ₂ profile	1 K	1 K
Weighted temperature		
AMF(O ₂ O ₂)	0.1 %	0.1 %
VCD*(O ₂ O ₂)	1.6 %	1.6 %
Δ SCD(O ₂ O ₂)	< 2 %	< 1 %
SCD _{ref} (O ₂ O ₂)	2.4 %	0.8 %
Total error	3.5 %	2.1 %
Aircraft MAX-DOAS		
O ₂ O ₂ profile	1 K	1 K
Weighted temperature		
Δ AMF(O ₂ O ₂)	0.4 %	0.4 %
VCD*(O ₂ O ₂)	0.8 %	0.8 %
Δ SCD(O ₂ O ₂)	3.8 %	2.0 %
SCD _{ref} (O ₂ O ₂)	< 6.8 % ^a < 3.5 % ^b	< 2.3 % ^a < 0.9 % ^b
Total error	< 5.2 %	< 2.4 %

^a Maximum relative error from Table 4; ^b maximum relative error weighed by the relative contribution of the SCD_{ref} to the overall; SCD = dSCD + SCD_{ref}; weighed relative error = (SCD_{ref}/SCD) · SCD_{ref,error}; the ratio SCD_{ref}/SCD is on average 0.51 and 0.39 at 360 and 477 nm, respectively.

4.6 Accounting for temperature dependence of measured $\tau(\text{O}_2\text{O}_2)$ in DOAS fitting

Given the relatively cold O₂O₂ effective temperatures of the AMAX-DOAS measurements (~ 231 – 244 K), results are expected to improve by simultaneous DOAS fitting of two $\sigma(\text{O}_2\text{O}_2)$ cross sections (Thalman and Volkamer, 2013) at 293 and 203 K. Figure 5 shows substantial reduction in

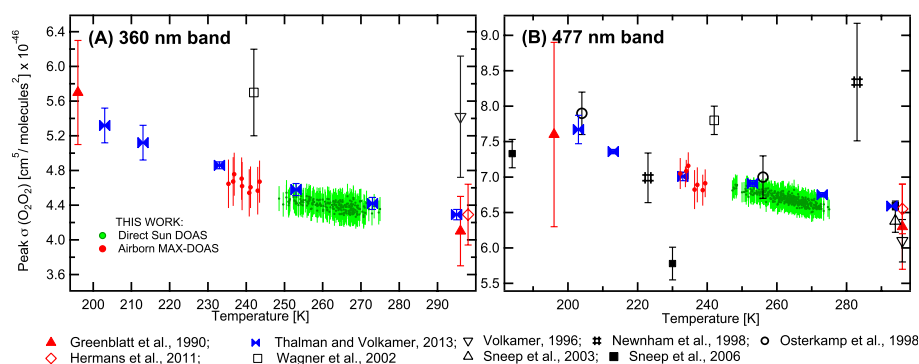


Figure 7. Collision-induced absorption cross section of O₂O₂ at 360 (a) and 477 nm (b), recorded in literature since 1990 at their corresponding spectral resolutions. DS and AMAX-DOAS-derived peak cross sections (THIS WORK) are scaled to 0.3 nm FWHM, using Hermans et al. (1999), 296 K.

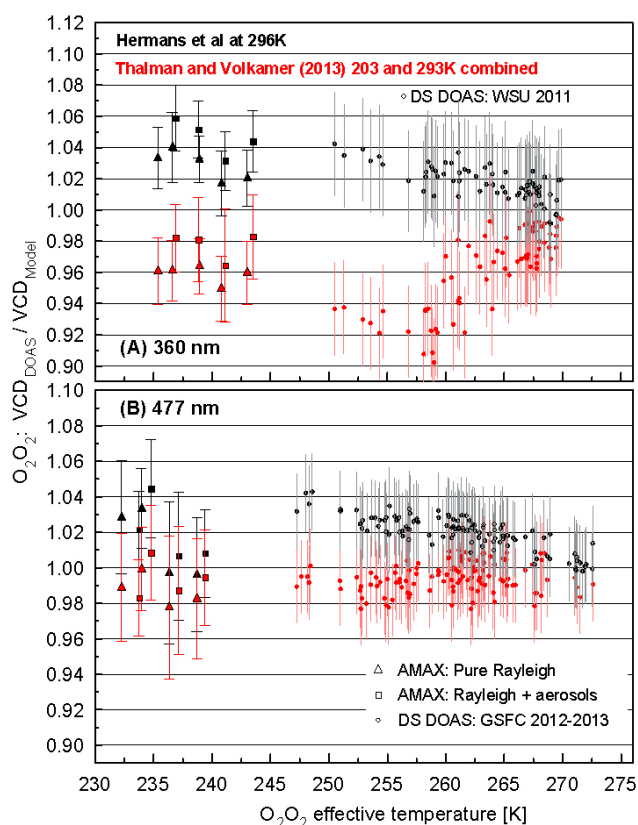


Figure 8. Ground-based DS and AMAX-DOAS-derived VCD from DOAS fitting in the UV (a) and visible (b) spectral windows using $\sigma(\text{O}_2\text{O}_2)$ by (1) Hermans et al. 296 (black symbols) and (2) Thalman and Volkamer (2013) at 203 and 293 K (red symbols) and normalized by VCD* calculated from model (AMAX) and measured T , P and SH profiles. DS UV spectra, collected with U340 filter, were analyzed using AMAX-DOAS settings (Table 3). AMAX-DOAS data are averaged and binned for 2 K increments for a pure Rayleigh atmosphere and including aerosols.

the residual OD structures as well as decreases in the fitted ΔSCD (203 and 293 K combined). This presents independent evidence from field observations that the spectral band shapes depend on temperature. Figure 3 and Table 4 also show the effect of more accurately accounting for the temperature dependence of σ on the correlation between AMAX-measured ΔSCD and modeled SCD. The results for Rayleigh and aerosol cases at 477 nm are comparable to fitting $\sigma(\text{O}_2\text{O}_2)$ at a single T within corresponding errors. The slopes are indistinguishable from unity and the SCD_{REF} are within less than 1 % of the modeled $\text{SCD}_{\text{REF}}^*$. Fitting two O₂O₂ cross sections has a more pronounced effect on the slope and SCD_{REF} at 360 nm. Derived slopes decrease both for pure Rayleigh and aerosol cases by about 7 %, which brings the slope for the aerosol case within 2 % of unity. While the temperature dependence in the combined ΔSCD vs. SCD^* is reduced, the recalculated SCD_{REF} is slightly underestimated (less than 7 % for pure Rayleigh case and 5 % for aerosol case).

Figure 8 shows measured VCD normalized by VCD* in the case of fitting one cross section (Hermans et al. at 296 K) and two cross sections (Thalman and Volkamer, 2013, at 203 and 293 K) for DS and AMAX-DOAS measurements at 360 nm (panel a) and 477 nm (panel b). The inverse of the normalized VCD can be interpreted as “correction factors” necessary to bring the measured VCDs to “true” VCD*. In the case of fitting a single σ at 296 K, the CFs are temperature dependent and range from 1 ± 0.02 at 275 K to 0.94 ± 0.02 at 231 K for both UV and visible spectral regions. The effect of temperature to bias the fitted $\Delta\text{SCD}(\text{O}_2\text{O}_2)$ is buffered by the fact that the integral O₂O₂ absorption (integral over the wavelength window of each spectral band) does not depend on temperature (Thalman and Volkamer, 2013). The temperature-induced corrections required to bring ground-based DS and aircraft AMAX-DOAS VCDs to the model values are significantly smaller than the corrections reported for the boundary layer MAX-DOAS observations in the literature (0.94 ± 0.02 vs. 0.75 ± 0.1 , see Table 1).

When making a DOAS fit using O₂O₂ cross sections at two temperatures (203 and 293 K), the temperature-dependent bias in the measured VCDs is essentially zero within errors at 477 nm. This illustrates the importance of (1) accounting for the temperature dependence of the O₂O₂ cross section during the DOAS fit and (2) accurately representing the atmosphere in the RTM (results including aerosol are better compared to the Rayleigh case due to some contribution of O₂O₂ absorption from low altitudes to the measurements at high altitude).

The UV region, however, is more sensitive to the DOAS fitting parameters and does not show a clear improvement in the retrieved VCDs while using O₂O₂ absorption cross sections at two temperatures (203 and 293 K). This is especially pronounced for DS measurements (Fig. 8), where several percent underestimation of the VCD is observed. AMAX-DOAS data seem to be less sensitive and show only a few percent underestimations that are insignificant compared to the low error bars.

4.7 Error analysis of ground-based DS and AMAX-DOAS data

4.7.1 Direct-sun DOAS errors

The main source of error in DS $\tau(\text{O}_2\text{O}_2)$ measurements is the DOAS fitting error of $\Delta\text{SCD}(\text{O}_2\text{O}_2)$. Since DS AMF(O₂O₂) is wavelength independent at most SZA, retrieval in any of the wavelength regions where O₂O₂ has a significant absorption should produce the same ΔSCD . In practice, DOAS fitting parameters, such as the order of the polynomial function, mimicking Rayleigh and Mie extinction, exact fitting window boundaries, offset correction, uncertainties in cross sections of other trace gases absorbing in the same wavelength region, errors in instrument transfer function and wavelength calibration, introduce errors in ΔSCD . Table 5 summarizes DS-normalized $\tau(\text{O}_2\text{O}_2)$ errors calculated for different DOAS fitting scenarios accounting for variability in CD.

An error associated with DS AMF comes from the uncertainty in SZA ephemeris and O₂O₂ effective height calculation. The error in the SZA calculation is 0.02° and error in the O₂O₂ effective height is less than 200 m. This translates to an AMF error of less than 0.1 % at SZA < 80°, which increases to 2 % at 88° SZA. Since most measurements contributing to the final results come from the observations at SZA < 80°, we assume an AMF error of 0.1 %.

Error in the total VCD* calculated from the T , P and SH profiles is determined as 1 standard deviation of VCD* variability at a specific T . The yearly average relative error is about 1.6 %.

To evaluate ΔSCD and SCD_{REF} errors associated with the DOAS fitting parameters, we varied the wavelength fitting windows (visible: 435–485, 445–485, 460–490; UV: 350–385, 350–370, 335–370, 335–390 nm), polynomial order (3,

4 and 5, depending on the $\Delta\lambda$), offset order (0 and 1), and $\sigma(\text{O}_3)$ (single temperature vs. two temperatures). One standard deviation of the SCD_{REF} derived from all fitting scenarios is reported as SCD_{REF} error. This is about 1 % for the visible spectral window and 2.4 % for the UV.

The noise in the residual OD (Eq. 3) was significantly reduced by averaging daily measurements, resulting in SNR increase between 5 and 27 times, depending on the observation schedule.

The total error in the normalized daily VOD and VCD is derived from the DOAS sensitivity scenarios and $\text{VCD}^* \pm 1.6\%$ as 1 standard deviation. It is about 3.5 % for the UV and 2.1 % for the visible wavelength regions.

4.7.2 Aircraft MAX-DOAS

The DOAS fitting error of $\Delta\text{SCD}(\text{O}_2\text{O}_2)$ is the main error source for the AMAX-DOAS data. Error values listed in Table 5 are representative of individual measurements with a 15 s time resolution. Statistical averaging of individual spectra can be used to further reduce this error. The total errors of 5.2 % at 360 nm and 2.4 % at 477 nm are therefore upper limits, particularly in the UV. AMAX-DOAS data shown in Figs. 6 and 8 are taken from EA 0° measurements only. Unlike for the DS measurements, Eq. (3) was directly applied to the AMAX-DOAS ΔSCD results without prior averaging. To reduce scatter, VOD and VCD data included in Figs. 6 and 8 are averages and standard deviations of binned data in 2 K increments. The AMF error is due to the statistical nature of the Monte Carlo RTM McArtim (statistical uncertainty). McArtim was initiated several times with identical settings and variations are small. The error in the total $\text{VCD}^*(\text{O}_2\text{O}_2)$ is directly representative of the error in our temperature measurements; errors due to pressure measurements are negligible. The major source of uncertainty is related to assumptions about SCD_{REF} . We assess this error by determining SCD_{REF} experimentally from the offsets of linear fits of measured $\Delta\text{SCD}(\text{O}_2\text{O}_2)$ over modeled $\text{SCD}(\text{O}_2\text{O}_2)$, as shown in Fig. 4 and detailed in Table 4. These offsets agree within error bars with those computed from RTM for a Rayleigh atmosphere or for an atmosphere containing aerosols (see Table 4).

The excellent agreement between ground-based DS DOAS (no RTM) and aircraft AMAX-DOAS (using RTM) is not trivial given the need for radiative transfer calculations and active control of telescope pointing with AMAX-DOAS observations (Baidar et al., 2013). For example, a 1 % uncertainty in the Rayleigh scattering cross section used in the RTM directly translates into an error of the same order in the predicted $\text{SCD}(\text{O}_2\text{O}_2)$. A recent laboratory study extends knowledge about Rayleigh scattering cross sections at UV wavelengths (Thalman et al., 2014) and confirms that the cross sections that underlie our RTM are correct within very small error bounds (< 1 %). This is noteworthy, since variations in the Rayleigh scattering cross sections had been found around 4 % at 477 nm when comparing empirical fits

of previous measurements in the literature to theory (Thalman et al., 2014). We conclude that any systematic bias from using the RTM to interpret the AMAX-DOAS measurements is not due to the representation of Rayleigh scattering, and is limited by the small remaining uncertainty due to aerosols. Missing knowledge on aerosol distribution and properties in the atmosphere presents a fundamental limitation to determining SCD_{REF} for AMAX-DOAS measurements.

The difference in SCD_{REF} between a Rayleigh or aerosol atmosphere introduces a systematic error of about 2 % in modeled VCD and VOD values (see Figs. 6 and 8). We consider this to be the limit at which our data can be considered accurate. The overall errors for both DS and AMAX-DOAS are comparable, particularly after averaging AMAX-DOAS Δ SCD(O₂O₂).

5 Summary

The main scope of this study is to evaluate O₂O₂ absorption optical depths (335–390 and 435–490 nm) under well-characterized atmospheric conditions using DOAS measurements with well-understood observation geometry (ground-based direct-sun and airborne MAX-DOAS). The data were evaluated to understand the temperature and pressure dependence of the O₂O₂ molecular absorption cross section using vertical O₂O₂ column densities calculated from atmospheric sounding, in situ data and/or model temperature and pressure profiles adjusted by the surface observations.

Based on the ground-based DS observations, there is no pressure dependence of the O₂O₂ cross section between 780 and 1011 hPa within instrumental errors (3 %). DS O₂O₂ absorption measurements “simulating” MAX-DOAS observations within lowest 2.2 km and 680 m and AMF ranging from 1.1 to 9 showed agreement with the theoretically calculated SCD to better than 4 %.

A temperature dependence in σ (O₂O₂) from 231 to 275 K was observed at about 9 % \pm 2.5 % per 44 K rate in both wavelength regions from DS and AMAX-DOAS measurements. The change in band shape described by Thalman and Volkamer (2013) was observed under atmospheric conditions in both ground-based DS and aircraft AMAX-DOAS data sets. Derived peak O₂O₂ cross sections of 360 and 477 nm bands were compared to the recent laboratory-measured O₂O₂ cross sections of Thalman and Volkamer (2013) at 233, 253 and 273 K. The agreement between the peak O₂O₂ cross sections at both wavelengths is within 3 %.

The combined observations of ground-based DS and aircraft AMAX-DOAS measurements support the fact that laboratory-measured O₂O₂ cross sections are well suited for DOAS observations under typical atmospheric conditions.

The effect of the σ (O₂O₂) temperature dependence on the fitted Δ SCD(O₂O₂) is buffered by the fact that the integral O₂O₂ absorption (integral over the wavelength window of each band) does not depend on temperature (Thalman

and Volkamer, 2013). SCD retrieved from DS and AMAX-DOAS measurements were within 6 % of the model T , P and SH even at temperatures below 250 K. This shows that the O₂O₂ cross section makes no contribution to the correction factors of $\sim 25 \pm 10$ % reported in the literature for (some) PBL MAX-DOAS measurements where the effective O₂O₂ temperatures are expected to be between 265 K (zenith) and 275 K (1–2° EA).

Temperature-dependent bias in Δ SCD can be reduced by simultaneously fitting σ (O₂O₂) at different temperatures, which becomes increasingly important for measurements with effective O₂O₂ temperatures below 250 K, as is the case for AMAX-DOAS measurements. Fitting σ (O₂O₂) at 203 and 293 K improved AMAX-DOAS results in both UV and visible wavelength regions.

Assessments of the accuracy of O₂O₂ OD measurements in the presence of aerosols have to date only been conducted under simulated atmospheric conditions for monodisperse aerosols of known refractive index. No need for a correction factor was observed (Thalman and Volkamer, 2010) (see their Fig. 8). Further investigation is needed to understand effects of atmospheric aerosol properties/distribution on RT modeling of O₂O₂ SCD and is beyond the scope of this paper.

Acknowledgements. The WSU MFDOAS instrument development and deployment were supported by National Aeronautics and Space Administration grants to Washington State University (NNX09AJ28G and NNG05GR56G). We thank the institutional support of the Jet Propulsion Laboratory Table Mountain Facility (Stanley Sander et al.); University of Alaska in Fairbanks (William Simpson et al.); NASA Goddard Space Flight Center; Cabauw, Netherlands (CINDI organizers); University of Alabama in Huntsville (M. Newchurch et al.); and Dept. of Energy Pacific Northwest National Laboratory, Richland, WA (Jim Mather et al.), where the various field measurements were made. Ozonesonde measurements were supported through NOAA.

The TORERO project is funded by the National Science Foundation AGS-1104104 (PI: R. Volkamer) awarded to CU. The involvement of the National Science Foundation-sponsored Lower Atmospheric Observing Facilities, managed and operated by the National Center for Atmospheric Research Earth Observing Laboratory, is acknowledged. RV acknowledges financial support from the NSF Faculty Early Career Development (CAREER) award ATM-0847793 to develop the CU AMAX-DOAS instrument. SB is the recipient of a ESRL/CIRES graduate fellowship. IO is the recipient of a NASA graduate fellowship. The authors thank Brad Pierce for RAQMS model data used to constrain McArtim and Tim Deutschman for providing McArtim.

Edited by: M. Van Roozendael

References

- Acarreta, J. R., De Haan, J. F., and Stammes, P.: Cloud pressure retrieval using the O₂-O₂ absorption band at 477 nm, *J. Geophys. Res.*, 109, D05204, doi:10.1029/2003JD003915, 2004.
- Baidar, S., Oetjen, H., Coburn, S., Dix, B., Ortega, I., Sinreich, R., and Volkamer, R.: The CU Airborne MAX-DOAS instrument: vertical profiling of aerosol extinction and trace gases, *Atmos. Meas. Tech.*, 6, 719–739, doi:10.5194/amt-6-719-2013, 2013.
- Bogumil, K.: Measurements of molecular absorption spectra with the SCIAMACHY pre-flight model: instrument characterization and reference data for atmospheric remote-sensing in the 230–2380 nm region, *J. Photochem. Photobiol. A: Chemistry*, 157, 167–184, doi:10.1016/S1010-6030(03)00062-5, 2003.
- Cede, A., Herman, J., Richter, A., Krotkov, N., and Burrows, J.: Measurements of nitrogen dioxide total column amounts using a Brewer double spectrophotometer in direct Sun mode, *J. Geophys. Res.*, 111, D05304, doi:10.1029/2005JD006585, 2006.
- Cl  mer, K., Van Roozendaal, M., Fayt, C., Hendrick, F., Hermans, C., Pinardi, G., Spurr, R., Wang, P., and De Mazi  re, M.: Multiple wavelength retrieval of tropospheric aerosol optical properties from MAXDOAS measurements in Beijing, *Atmos. Meas. Tech.*, 3, 863–878, doi:10.5194/amt-3-863-2010, 2010.
- Danckaert, T., Fayt, C., Van Roozendaal, M., De Smedt, I., Letocart, V., Merlaud, A., and Pinardi, G.: QDOAS Software User Manual, Belgian Institute for Space Aeronomy (BIRA-IASB), 2012.
- Daumont, D., Brion, J., Charbonnier, J., and Malicet, J.: Ozone UV spectroscopy I: Absorption cross-sections at room temperature, *J. Atmos. Chem.*, 15, 145–155, doi:10.1007/BF00053756, 1992.
- Denning, R. F., Guidero, S. L., Parks, G. S., and Gary, B. L.: Instrument description of the airborne microwave temperature profiler, *J. Geophys. Res.*, 94, 16757, doi:10.1029/JD094iD14p16757, 1989.
- Deutschmann, T., Beirle, S., Frie  , U., Grzegorski, M., Kern, C., Kritten, L., Platt, U., Prados-Rom  n, C., Pu    te, J., Wagner, T., Werner, B., and Pfeilsticker, K.: The Monte Carlo atmospheric radiative transfer model McArtim: Introduction and validation of Jacobians and 3D features, *J. Q. Spectr. Radiat. T.*, 112, 1119–1137, doi:10.1016/j.jqsrt.2010.12.009, 2011.
- Dix, B., Baidar, S., Bresch, J. F., Hall, S. R., Schmidt, K. S., Wang, S., and Volkamer, R.: Detection of iodine monoxide in the tropical free troposphere, *Proc. Natl. Acad. Sci.*, 110, 2035–2040, doi:10.1073/pnas.1212386110, 2013.
- Eloranta, E. W., Razenkov, I. A., Hedrick, J., and Garcia, J. P.: The Design and Construction of an Airborne High Spectral Resolution Lidar, pp. 1–6, IEEE, 2008.
- Fayt, C. and Van Roozendaal, M.: WinDOAS 2.1 Software User Manual, BIRA-IASB, Uccle, Belgium, 2001.
- Fleischmann, O. C., Hartmann, M., Burrows, J. P., and Orphal, J.: New ultraviolet absorption cross-sections of BrO at atmospheric temperatures measured by time-windowing Fourier transform spectroscopy, *J. Photochem. Photobiol. A: Chemistry*, 168, 117–132, doi:10.1016/j.jphotochem.2004.03.026, 2004.
- Frie  , U., Monks, P. S., Remedios, J. J., Rozanov, A., Sinreich, R., Wagner, T., and Platt, U.: MAX-DOAS O₄ measurements: A new technique to derive information on atmospheric aerosols: 2. Modeling studies, *J. Geophys. Res.*, 111, D17S90, doi:10.1029/2005JD006618, 2006.
- Greenblatt, G. D., Orlando, J. J., Burkholder, J. B., and Ravishankara, A. R.: Absorption Measurements of Oxygen Betwe-
- tween 330 and 1140 nm, *J. Geophys. Res.*, 95, 18577–18582, doi:10.1029/JD095iD11p18577, 1990.
- Herman, J., Cede, A., Spinei, E., Mount, G., Tzortziou, M., and Abuhassan, N.: NO₂ column amounts from groundbased Pandora and MFDOAS spectrometers using the direct-sun DOAS technique: Intercomparisons and application to OMI validation, *J. Geophys. Res.*, 114, D13307, doi:10.1029/2009JD011848, 2009.
- Hermans, C.: O₄ absorption cross-sections at 296 K (335.59–666.63 nm), online available from: <http://spectrolab.aeronomie.be/index.htm> (last accessed 15 January 2011), 2011.
- Hermans, C., Vandaele, A., Carleer, M., Fally, S., Colin, R., Jenouvrier, A., Coquart, B., and M  rienne, M.-F.: Absorption cross-sections of atmospheric constituents: NO₂, O₂, and H₂O, *Environ. Sci. Pollut. Res.*, 6, 151–158, doi:10.1007/BF02987620, 1999.
- Irie, H., Kanaya, Y., Akimoto, H., Iwabuchi, H., Shimizu, A., and Aoki, K.: First retrieval of tropospheric aerosol profiles using MAX-DOAS and comparison with lidar and sky radiometer measurements, *Atmos. Chem. Phys.*, 8, 341–350, doi:10.5194/acp-8-341-2008, 2008.
- Irie, H., Kanaya, Y., Akimoto, H., Iwabuchi, H., Shimizu, A., and Aoki, K.: Dual-wavelength aerosol vertical profile measurements by MAX-DOAS at Tsukuba, Japan, *Atmos. Chem. Phys.*, 9, 2741–2749, doi:10.5194/acp-9-2741-2009, 2009.
- Irie, H., Takashima, H., Kanaya, Y., Boersma, K. F., Gast, L., Witrock, F., Brunner, D., Zhou, Y., and Van Roozendaal, M.: Eight-component retrievals from ground-based MAX-DOAS observations, *Atmos. Meas. Tech.*, 4, 1027–1044, doi:10.5194/amt-4-1027-2011, 2011.
- Langley, S. P.: The bolometer and radiant energy, *Proc. American Acad. Arts and Sciences*, 16, 342–358, 1881.
- Lim, B., Mahoney, M., Haggerty, J., and Denning, R.: The Microwave Temperature Profiler performance in recent airborne campaigns, *IEEE*, pp. 3363–3366, 2013.
- Malicet, J., Daumont, D., Charbonnier, J., Parisse, C., Chakir, A., and Brion, J.: Ozone UV spectroscopy. II. Absorption cross-sections and temperature dependence, *J. Atmos. Chem.*, 21, 263–273, doi:10.1007/BF00696758, 1995.
- Massie, S. T. and Hervig, M.: HITRAN 2012 refractive indices, *J. Q. Spectr. Radiat. T.*, 130, 373–380, doi:10.1016/j.jqsrt.2013.06.022, 2013.
- Meller, R. and Moortgat, G. K.: Temperature dependence of the absorption cross sections of formaldehyde between 223 and 323 K in the wavelength range 225–375 nm, *J. Geophys. Res.*, 105, 7089–7101, doi:10.1029/1999JD901074, 2000.
- Merlaud, A., Van Roozendaal, M., Theys, N., Fayt, C., Hermans, C., Quennehen, B., Schwarzenboeck, A., Ancellet, G., Pommier, M., Pelon, J., Burkhardt, J., Stohl, A., and De Mazi  re, M.: Airborne DOAS measurements in Arctic: vertical distributions of aerosol extinction coefficient and NO₂ concentration, *Atmos. Chem. Phys.*, 11, 9219–9236, doi:10.5194/acp-11-9219-2011, 2011.
- Newnham, D. A. and Ballard, J.: Visible absorption cross sections and integrated absorption intensities of molecular oxygen (O₂ and O₄), *J. Geophys. Res.*, 103, 28801–28815, doi:10.1029/98JD02799, 1998.
- Osterkamp, H., Ferlemann, F., Harder, H., Perner, D., Platt, U., and Schneider, M.: First measurement of the atmospheric O₄ profile, in: *Proceedings of the 4th European Symposium on Polar*

- stratospheric ozone 1997, Schliersee/Germany, pp. 478–481, Luxembourg: European Commission, 1998.
- Pfeilsticker, K., Bösch, H., Camy-Peyret, C., Fitzenberger, R., Harder, H., and Osterkamp, H.: First atmospheric profile measurements of UV/visible O₄ absorption band intensities: Implications for the spectroscopy, and the formation enthalpy of the O₂O₂ dimer, *Geophys. Res. Lett.*, 28, 4595, doi:10.1029/2001GL013734, 2001.
- Pierce, R. B., Schaack, T., Al-Saadi, J. A., Fairlie, T. D., Kitaka, C., Lingenfelter, G., Natarajan, M., Olson, J., Soja, A., Zapotocny, T., Lenzen, A., Stobie, J., Johnson, D., Avery, M. A., Sachse, G. W., Thompson, A., Cohen, R., Dibb, J. E., Crawford, J., Rault, D., Martin, R., Szykman, J. and Fishman, J.: Chemical data assimilation estimates of continental U.S. ozone and nitrogen budgets during the Intercontinental Chemical Transport Experiment – North America, *J. Geophys. Res.*, 112, doi:10.1029/2006JD007722, 2007.
- Platt, U.: Differential Optical Absorption Spectroscopy (DOAS), in: *Air monitoring by spectroscopic techniques*, vol. 127, edited by: Sigrist, M. W., p. 531, Wiley-IEEE, New York, 1994.
- Rothman, L. S., Gordon, I. E., Barber, R. J., Dothe, H., Gamache, R. R., Goldman, A., Perevalov, V. I., Tashkun, S. A., and Tennyson, J.: HITRAN, the high-temperature molecular spectroscopic database, *J. Q. Spectr. Radiat. T.*, 111, 2139–2150, doi:10.1016/j.jqsrt.2010.05.001, 2010.
- Salow, H. and Steiner, W.: Absorption Spectrum of Oxygen at High Pressures and the Existence of O₄ Molecules, *Nature*, 134, 463–463, doi:10.1038/134463a0, 1934.
- Sneep, M. and Ubachs, W.: Cavity ring-down measurement of the O₂-O₂ collision-induced absorption resonance at 477 nm at sub-atmospheric pressures, *J. Q. Spectr. Radiat. T.*, 78, 171–178, doi:10.1016/S0022-4073(02)00190-5, 2003.
- Sneep, M., Ityaksov, D., Aben, I., Linnartz, H., and Ubachs, W.: Temperature-dependent cross sections of O₂-O₂ collision-induced absorption resonances at 477 and 577 nm, *J. Q. Spectr. Radiat. T.*, 98, 405–424, doi:10.1016/j.jqsrt.2005.06.004, 2006.
- Sneep, M., de Haan, J. F., Stammes, P., Wang, P., Vanbaune, C., Joiner, J., Vasilkov, A. P., and Levelt, P. F.: Three-way comparison between OMI and PARASOL cloud pressure products, *J. Geophys. Res.*, 113, D15S23, doi:10.1029/2007JD008694, 2008.
- Thalman, R. and Volkamer, R.: Inherent calibration of a blue LED-CE-DOAS instrument to measure iodine oxide, glyoxal, methyl glyoxal, nitrogen dioxide, water vapour and aerosol extinction in open cavity mode, *Atmos. Meas. Tech.*, 3, 1797–1814, doi:10.5194/amt-3-1797-2010, 2010.
- Thalman, R. and Volkamer, R.: Temperature dependent absorption cross-sections of O₂-O₂ collision pairs between 340 and 630 nm and at atmospherically relevant pressure, *Phys. Chem. Chem. Phys.*, 15, 15371, doi:10.1039/c3cp50968k, 2013.
- Thalman, R., Zarzana, K. J., Tolbert, M. A., and Volkamer, R.: Rayleigh scattering cross-section measurements of nitrogen, argon, oxygen and air, *J. Quant. Spectr. Radiat. T.*, 147, 171–177, doi:10.1016/j.jqsrt.2014.05.030, 2014.
- Vandaele, A., Hermans, C., Simon, P., Carleer, M., Colin, R., Fally, S., Mérienne, M.-F., Jenouvrier, A., and Coquart, B.: Measurements of the NO₂ absorption cross-section from 42 000 cm⁻¹ to 10 000 cm⁻¹ (238–1000 nm) at 220 K and 294 K, *J. Q. Spectr. Radiat. T.*, 59, 171–184, doi:10.1016/S0022-4073(97)00168-4, 1998.
- Vandaele, A. C., Hermans, C., Fally, S., Carleer, M., Mérienne, M.-F., Jenouvrier, A., Coquart, B., and Colin, R.: Absorption cross-sections of NO₂: simulation of temperature and pressure effects, *J. Q. Spectr. Radiat. T.*, 76, 373–391, doi:10.1016/S0022-4073(02)00064-X, 2003.
- Vlemmix, T., Piders, A. J. M., Berkhout, A. J. C., Gast, L. F. L., Wang, P., and Levelt, P. F.: Ability of the MAX-DOAS method to derive profile information for NO₂: can the boundary layer and free troposphere be separated?, *Atmos. Meas. Tech.*, 4, 2659–2684, doi:10.5194/amt-4-2659-2011, 2011.
- Volkamer, R.: Absorption von Sauerstoff im Herzberg I System und Anwendungen auf die Aromatenmessungen am EUROPRAN PHOTOREACTOR (EUPHORE), Diploma thesis, Univ. of Heidelberg, Germany, 1996.
- Wagner, T., Friedeburg, C. von, Wenig, M., Otten, C., and Platt, U.: UV-visible observations of atmospheric O₄ absorptions using direct moonlight and zenith-scattered sunlight for clear-sky and cloudy sky conditions, *J. Geophys. Res.*, 107, 4424, doi:10.1029/2001JD001026, 2002.
- Wagner, T., Dix, B., Friedeburg, C. v., Frieß, U., Sanghavi, S., Sinreich, R., and Platt, U.: MAX-DOAS O₄ measurements: A new technique to derive information on atmospheric aerosols-Principles and information content, *J. Geophys. Res.-Atmos.*, 109, 22205, doi:10.1029/2004JD004904, 2004.
- Wagner, T., Deutschmann, T., and Platt, U.: Determination of aerosol properties from MAX-DOAS observations of the Ring effect, *Atmos. Meas. Tech.*, 2, 495–512, doi:10.5194/amt-2-495-2009, 2009.
- Wilmouth, D. M., Hanisco, T. F., Donahue, N. M., and Anderson, J. G.: Fourier Transform Ultraviolet Spectroscopy of the A²Π_{3/2} ← X²Π_{3/2} Transition of BrO⁺, *J. Phys. Chem. A*, 103, 8935–8945, doi:10.1021/jp991651o, 1999.
- Zieger, P., Weingartner, E., Henzing, J., Moerman, M., de Leeuw, G., Mikkilä, J., Ehn, M., Petäjä, T., Clémer, K., van Roozendael, M., Yilmaz, S., Frieß, U., Irie, H., Wagner, T., Shaiganfar, R., Beirle, S., Apituley, A., Wilson, K., and Baltensperger, U.: Comparison of ambient aerosol extinction coefficients obtained from in-situ, MAX-DOAS and LIDAR measurements at Cabauw, *Atmos. Chem. Phys.*, 11, 2603–2624, doi:10.5194/acp-11-2603-2011, 2011.